

INTERACTION OF FREESTREAM TURBULENCE WITH VORTEX STRUCTURES IN VERTICAL AXIS TURBINES

Jovan Nedić
Mechanical Engineering
McGill University
Montréal, Canada
jovan.nedic@mcgill.ca

Daniel Fernex
Mechanical Engineering
EPFL
Lausanne, Switzerland
daniel.fernex@epfl.ch

Karen Mulleners
Mechanical Engineering
EPFL
Lausanne, Switzerland
karen.mulleners@epfl.ch

ABSTRACT

We investigate the performance of an H-type vertical axis turbine in a turbulent freestream, focusing on the interaction of the turbulence with the vortical structures created by the turbine. Emphasis is placed on understanding the combined effects of turbulence intensity in the freestream and the turbulence integral scale relative to the generated vortices. A series of regular grids, creating turbulence intensity levels ranging from 3 % to 12 %, and turbulent integral scales that are comparable in size to the leading edge vortex, are placed upstream of the turbine. Turbulence is found to generally increase the performance of the turbine by roughly 30% for tip-speed ratios below the optimal case in a laminar flow. Freestream turbulence was found to generally weaken the leading edge vortex, but also increased the standard deviation of the total forces on the blade.

INTRODUCTION

Vertical axis or cross-flow turbines are a promising solution to sustainable onshore power generation, particularly in urban environments, owing to their small footprint, low manufacturing and operational costs, low noise levels, and omnidirectional operational capabilities. In an urban environment, these turbines experience time-varying wind directions and non-negligible turbulence levels similar to those experienced by horizontal axis turbines in wind farms. The community has primarily focused on understanding the effects of freestream turbulence on the performance of horizontal axis turbines. Vertical axis turbines have received less attention. This lack of understanding might inhibit the widespread adoption of vertical axis turbines on a commercial scale (Kumar *et al.*, 2018).

Although sparse in number, previous studies have consistently shown that increasing turbulence intensity $T_u = u_{\text{rms}}/U_\infty$ (ratio of the root-mean-square velocity to the freestream velocity) increases the power output of a vertical axis turbine (Ahmadi-Baloutaki *et al.*, 2015; Peng & Lam, 2016; Peng *et al.*, 2019; Molina *et al.*, 2019; Belabes & Paraschivoiu, 2021). Ahmadi-Baloutaki *et al.* (2015) showed that the turbine power output increases by one order of magnitude when the turbulence level is increased from 0.5 % (laminar case) to 5 %. A further increase in the turbulence levels to 7.5 % and 10 % did not lead to a further increase in performance. Peng & Lam (2016) verified these conclusions and showed that freestream turbulence decreases the self-starting velocity of the turbine. The increase in turbine performance is attributed to the interaction of the freestream with the boundary layer on the wing,

which delays stall and increases the average thrust across the rotation cycle. Similar observations have been made for static wings (Hoffmann, 1991; Damiola *et al.*, 2023). Interestingly, the effect of turbulence intensity on turbine performance is prominent when compared to the laminar case. As the size of the turbine and the operational Reynolds number increase, the effect becomes negligible, and there is no overall change in performance in a turbulent freestream (Möllerström *et al.*, 2016; Belabes & Paraschivoiu, 2021). The turbine's resilience in a turbulent freestream is a notable result and further justifies why these turbines suit urban environments.

The nature of turbulence can not be modelled by its relative fluctuations alone. It must also include information about the size of the most energetic structures *i.e.*, the integral scale L_x . Peng *et al.* (2019) varied the integral scale from approximately $L_x=0.5c$ to $4c$ at a fixed intensity of 13 % and analyzed the impact on a 5-bladed H-type turbine. The same increase in performance due to freestream turbulence was observed. The increase in performance diminished as the integral scale was increased (note the performance was still better than the laminar case, even at the largest integral scale). Molina *et al.* (2019) could not discern any appreciable change in performance due to a change in integral scale. However, they could not keep the turbulence intensity fixed and vary the integral scale as was done in Peng *et al.* (2019).

In both studies, the analysis focused on the turbine's performance, and we lack knowledge of how the flow around the turbine is affected by a change in turbulence intensity and integral scale. The effects of integral scale on the turbine performance warrant further study, firstly to clarify how and secondly to understand why the performance is affected. We postulate that the turbine performance is tied to the interaction of the vortices generated by the blade with the energetic structures in the turbulent freestream. These vortices influence the lift generated by a single blade and the performance of a downstream blade as it advects towards them. We assume that the critical length scale of interest is the size of the vortex, as opposed to the blade's chord (although the size of this structure is expected to scale with the chord). We propose to systematically study the effect of both turbulence intensity and integral scale, as a function of the vortex size.

EXPERIMENTAL APPROACH

We tested the performance of a one-bladed H-type turbine model in a water tunnel. The blade has a NACA0018 profile, a chord of $c = 60$ mm, and a span of $s = 150$ mm. The

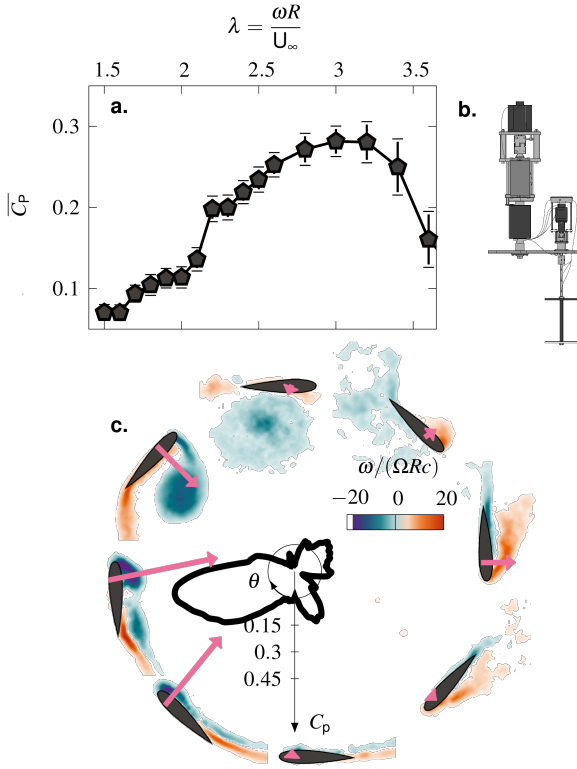


Figure 1: Baseline flow conditions and wind turbine prototype. (a) Evolution of the power coefficient $\overline{C_p}$ as a function of the tip-speed ratio λ . The power production peak of $C_p = 0.28$ is reached at $\lambda = 3.2$. (b) Experimental setup of the one-bladed vertical-axis wind turbine. (c) Azimuthal evolution of the vorticity field around the blade and the power coefficient. The onset of the leading edge vortex growth and its separation are visible in the upwind half.

turbine has a diameter of $D = 300$ mm, yielding a chord-to-diameter ratio of $c/D = 0.2$. A sketch of the prototype is shown in fig. 1b. The centre of the co-ordinate system coincides with the centre of the turbine and the positive stream-wise direction is defined in the downstream direction. The rotation of the blade is in the clockwise direction, with $\theta = 0^\circ$ defined such that the blade is at $x_t = 0D$, $y_t = -0.5D$, and $\theta = 90^\circ$ when at $x_t = -0.5D$, $y_t = 0D$. We kept the rotational speed of the turbine constant at $\omega R = 0.84 \text{ m s}^{-1}$ and systematically varied the water channel's flow velocity from 0.14 m s^{-1} to 0.70 m s^{-1} to obtain tip-speed ratios $\lambda = \omega R / U_\infty$ ranging from 1.2 to 4. The Reynolds number, based on the rotational speed, was constant at $\text{Re} = \omega R c / \nu \approx 50000$. Velocity measurements around the blade were taken using particle image velocimetry (PIV), where the field of view was centred on the blade itself (Le Fouest & Mulleners, 2022). Based on preliminary results (discussed below), three sets of regular grids were designed with a mesh size of $M = 45$ mm, 90 mm, and 180 mm each having a solidity (solid frontal area to test-section area) of 30%. These mesh sizes correspond to $M/c = 0.75$, 1.5 and 3 respectively. All three grids were placed 1265 mm upstream of the centre of the turbine. Across its diameter, the turbine is therefore subjected to grid-generated turbulence at normalised distances from the grid of $24.8 \leq x_g/M \leq 31.4$,

$12.4 \leq x_g/M \leq 15.7$, and $6.2 \leq x_g/M \leq 7.9$ for the grids with mesh sizes 45 mm, 90 mm, and 180 mm respectively. The properties of the generated turbulent flow at the upstream end of the turbine were measured using PIV.

TURBINE PERFORMANCE IN BASELINE FLOW

The power coefficient as a function of the tip-speed ratio for the turbine in a laminar flow is shown in fig. 1a. The power coefficient increases from $C_p = 0.07$ at $\lambda = 1.5$ to $C_p = 0.28$ at $\lambda = 3.2$, and decreases at higher tip-speed ratios. Below $\lambda = 2.2$, the wind turbine operates in a deep stall regime (Le Fouest & Mulleners, 2022), which explains the low efficiency in this region. The large and coherent leading-edge stall vortex initially creates a power performance peak, but its detachment from the blade yields massive flow separation, an efficiency drop, and detrimental blade-vortex interactions. At $\lambda > 2.2$, the blade undergoes light stall, with vastly decreased adverse effects. The smaller leading edge vortex enables higher power production, and the load transients caused by the flow separation are reduced.

The phase averaged vorticity field in the deep stall regime ($\lambda = 1.5$) at eight phase angles of interest are shown in fig. 1c. The black arrows indicate the direction and magnitude of the total force, and the flow is coming from the left. When the blade faces the incoming flow (bottom panel), the flow is attached. As the blade rotates, vorticity accumulates at the leading edge, and the shear layer rolls up, eventually forming a coherent stall vortex. The vortex reaches a size of the same magnitude as the chord length before it separates and is convected downstream (top panel). In the downwind half, the out-board side becomes the suction side, and the vorticity accumulates into a smaller leading edge vortex, which does not have as much time to grow as during the upwind half. The central black curve in fig. 1c shows the azimuthal evolution of C_p . The power production is mainly achieved in the upwind half. The black curve indicates a large lobe of power production during the onset of stall. As soon as the vortex pinches off from the surface, C_p drops sharply, and the blade barely produces power during the remainder of the rotation.

GRID TURBULENCE CHARACTERISATION

Three tip-speed ratios are chosen to study the performance of the turbine under turbulent conditions: $\lambda = 2$, 2.5, and 3. These correspond to conditions where the large scale vortex structures are diminishing in the baseline flow, and where the power coefficient is increasing up until a peak value at $\lambda = 3$.

The normalised streamwise velocity, \overline{u}/U_∞ (not shown here for brevity), for the three tip-speed ratios, and for each of the grids, as well as the baseline case are approximately constant, varying by 2% at most. In the lateral direction, a clear variation in mean flow is observed for the grid with the largest mesh size. The effect is largest for the highest tip-speed ratio case (lowest freestream velocity).

The variation of the streamwise turbulence intensity $T_u = u_{\text{rms}}/U_\infty$, along the streamwise and lateral direction are shown in fig. 2. Along the streamwise direction, the turbulence intensity decays for all turbulence grids and tip-speed ratios, with the turbulence intensity changing by approximately 1% across the measurement domain. Taking the data at $x_t = -0.5D$, $y_t = 0D$ as a reference point, which is the most upstream location of the blade, we find that the turbulence intensity approximately doubles as the mesh size doubles, increasing from $\approx 3.2\%$ for

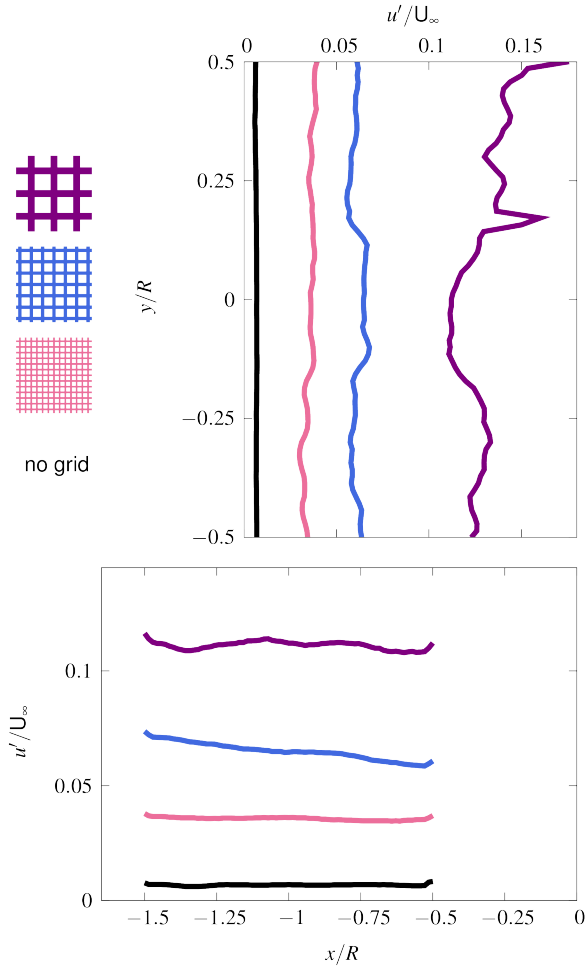


Figure 2: Variation of the streamwise turbulence intensity: top - in the lateral direction along $x_t = -0.5D$; bottom - in the streamwise direction along $y_t = 0D$.

the 45 mm mesh size grid, to $\approx 6.5\%$ for the 90 mm mesh size grid, and $\approx 12.3\%$ for the 180 mm mesh size grid. The footprint of the largest mesh size grid is still visible in the turbulence intensity profiles. The distance between the two peaks in fig. 2a for the largest mesh size grid corresponds to the mesh size of the grid. This is expected and consistent with similar results for grid-generated turbulence (Nedić & Tavoularis, 2016), where jet- and wake-like velocity profiles are observed for regions in front of open sections and solid bars of the grid, when $x_g < 30M$.

In fig. 2b, we observe no systematic variation in the lateral direction, and consider the turbulence to be approximately homogeneous. Given the finite streamwise distance over which the decaying turbulence was measured, the decay exponent for the turbulence intensity is not calculated. Even for the largest mesh size grid, which showed noticeable variation in the mean flow along the lateral direction, no such variation is present here. The lateral turbulence intensity $T_v = v_{rms}/U_\infty$ (not shown here for brevity) exhibited similar features. The large-scale isotropy, that is to say u_{rms}/v_{rms} , was found to lie between 1.1 and 1.5, indicating that the streamwise turbulence intensity is consistently higher than the lateral turbulence intensity. For the reference location of $x_t = -0.5D, y_t = 0D$, $T_v \approx 2.5\%$ for the 45 mm mesh size grid, $\approx 5\%$ for the 90 mm mesh size grid, and $\approx 11\%$ for the 180 mm mesh size grid. For the baseline case, i.e. no turbulence grid, the baseline turbulence intensity

is approximately 1%.

The streamwise integral scale, of the streamwise velocity, $L_{11,1}$, is defined as the integral of the correlation function of the streamwise velocity fluctuations $u' = u - \bar{U}$, where u is the instantaneous velocity and \bar{U} is the average velocity. Since the spatial correlation may not reduce to zero at certain locations within the chosen field of view, the integral scale was calculated by first calculating the spatial correlation coefficient

$$\rho(\mathbf{X}, r_1) = \frac{\overline{u'(\mathbf{X} - r_1/2)u'(\mathbf{X} + r_1/2)}}{\overline{u'(\mathbf{X})^2}} \quad (1)$$

where r_1 is the separation distance in the streamwise direction about the centroid position \mathbf{X} . The results from eq. (1) is then fitted with the function $f(r_1) = \exp^{-ar_1}$, whose integral is simply $1/a$. The integral scale is thus given by $L_{11,1} = 1/a$. At the reference point $\mathbf{X} = (-0.5D, 0D)$, the integral scales are $L_{11,1} \approx 38$ mm for the 45 mm mesh size grid, ≈ 40 mm for the 90 mm mesh size grid, and ≈ 57 mm for the 180 mm mesh size grid. Relative to the blade chord, this corresponds to $L_{11,1}/c \approx 0.63, 0.66,$ and 0.95 for the 45 mm, 90 mm, and 180 mm mesh size grids respectively. Relative to the size of the leading edge vortex that forms on the upstream blade, the integral scale is slightly larger.

TURBINE PERFORMANCE IN TURBULENT FLOW

Loads and power output

In fig. 3, the effects of the grids on the performance of the turbine are shown. At $\lambda = 3$, there is no discernible change in performance. As the tip speed ratio decreases, the power coefficient increases slightly. At first glance, these results suggest that at optimal operational conditions, where \bar{C}_p is maximum, turbulence has negligible effect. Turbulence appears to have more influence at sub-optimal tip speed ratios.

For $\lambda = 2.5$, \bar{C}_p systematically increases as the turbulence intensity increases, from $\bar{C}_p = 0.23$ for the laminar case, to 0.3 when the freestream intensity is about 12% (largest mesh size grid). A roughly similar effect is observed for the $\lambda = 2$ case, where a roughly 35% increase in \bar{C}_p is detected as the turbulence intensity is increased to 12%.

The middle and right plots of fig. 3 show the change in performance of the turbine over the upwind (middle) and downwind (right) part of the cycle. As expected, for all freestream conditions, the majority of the power generation comes from the upwind portion of the cycle. Interestingly, for $\lambda = 3$, we now see that the effects of turbulence generally increase the power generated in the upwind portion of the cycle, but that most of the gain is lost during the downwind portion. For $\lambda = 2.5$, freestream turbulence generally appears to increase the performance for both the upstream and downstream portion of the cycle.

Because the largest change in performance is observed for $\lambda = 2.5$, we will focus the remainder of our analysis on this condition. In fig. 4, we show the polar variation of the power coefficient (left), the total force coefficient (middle), and the standard deviation of the total force (right), for all freestream cases, for $\lambda = 2.5$.

The freestream turbulence increases the power output for $60^\circ \leq \theta \leq 100^\circ$, and for $315^\circ \leq \theta \leq 360^\circ$ (fig. 4). Recall that at $\theta = 0^\circ$, the blade is directly facing and aligned with the incoming flow. The vast majority of the total force is generated in the upwind portion of the rotation (fig. 4b). The total

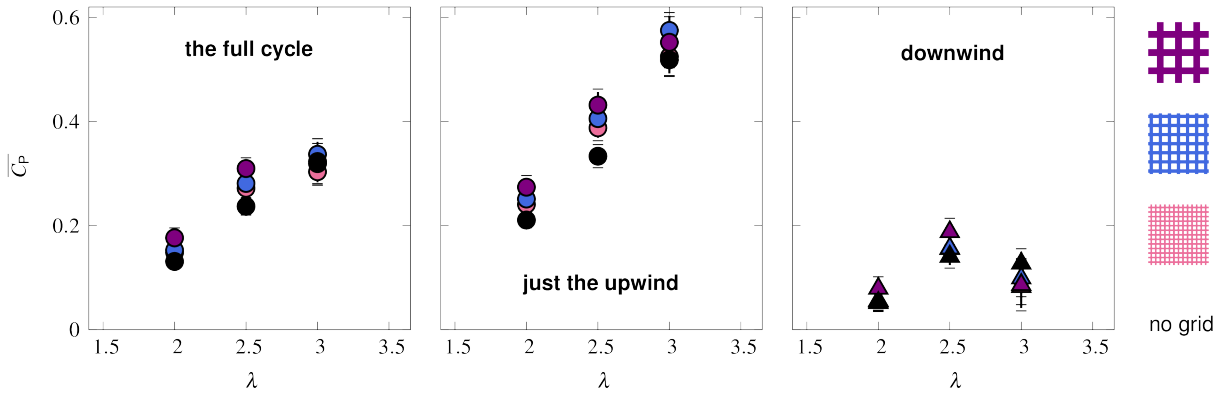


Figure 3: Change in power coefficient $\overline{C_p}$ as a function of tip speed ratio λ . Left - for the full cycle; middle - just the upwind half of the cycle; right - the downwind portion of the cycle.

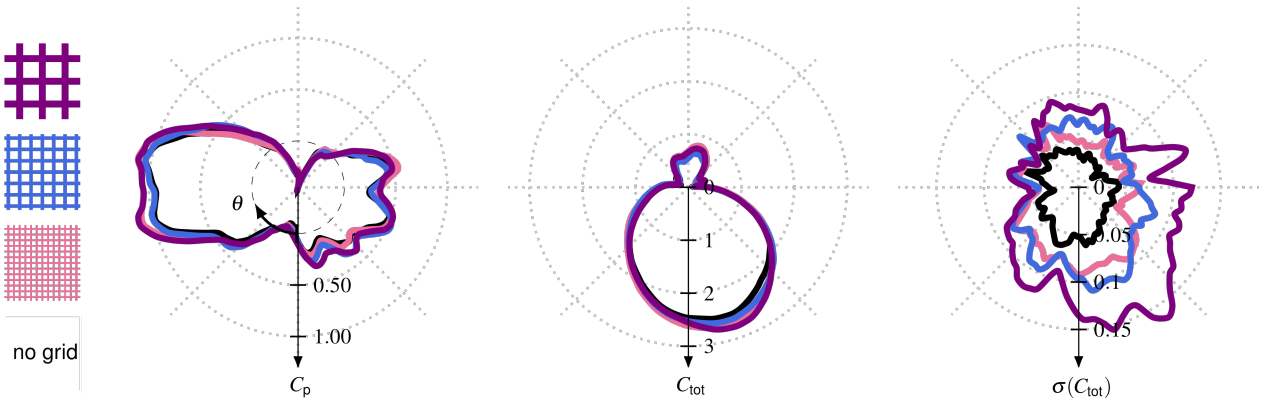


Figure 4: Polar variation of the: (left) power coefficient; (middle) total power coefficient C_{tot} ; (right) standard deviation of the total power $\sigma(C_{tot})$. Tip speed ratio is $\lambda = 2.5$.

force coefficient remains relatively unchanged across all angles and turbulence intensities, with the obvious exception for $315^\circ \leq \theta \leq 360^\circ$, where the total force coefficient increases as turbulence intensity increases from 3%, to 6%, to 12%. This corresponds to the region where the blade is approaching the upwind stroke and an increase in power output is observed as turbulence intensity increases.

The most striking effect of freestream turbulence is on the standard deviation of the total force coefficient (fig. 4c). A clear systematic increase in standard deviation can be observed as the freestream levels increase from 3%, to 6%, to 12%. This increase is non-negligible, with the standard deviation increasing by a factor of three between the laminar case and the 12% freestream turbulence case. The largest increase in standard deviation is observed at the end of the downwind, namely $315^\circ \leq \theta \leq 360^\circ$, which is also where the largest increase in total force coefficient and an increase in the power coefficient was observed.

Evidently, apart from increasing the overall power output at this particular tip speed ratio, the addition of freestream turbulence also increase the total force coefficient and its standard deviation. The latter is particularly important when it comes to considering the structural fatigue of the blade during operation. High fluctuations in the loads on the blade can lead to early structural failure.

Phased-averaged flow

Phased-averaged vorticity plots for $\lambda = 2.5$ are presented in fig. 5. For the laminar case, as the blade moves from $\theta = 80^\circ$ to $\theta = 212^\circ$, a large leading edge vortex is created, growing in size until its size has reached approximately half the chord length. By $\theta = 180^\circ$, the leading edge vortex has lifted off the surface, which corresponds to the large drop in $\overline{C_p}$ that was observed in fig. 3. The vortex then begins to move downstream, diffusing as it does so.

With the addition of turbulence in the freestream, the general features of the phased averaged flow remain relatively unchanged. A large leading edge vortex forms between $80^\circ \leq \theta \leq 160^\circ$, which then detaches around $\theta = 180^\circ$, and is advected downstream. At approximately $\theta = 80^\circ$, where we see the largest increase in power output with the addition of turbulence (fig. 3), there are no clear changes in the vorticity distribution. It is possible that the effects of turbulence at this particular phase of the rotation are confined to the near wall region, for which our experiments do not have sufficient resolution to resolve. The only observable change is the decrease in angle at which the shear layer leaves the trailing edge as the turbulence levels increase, which would result in a slight increase in effective angle of attack and power production.

At later phases of the rotation, the cumulative effects of freestream turbulence, although slight in nature, begin to appear. Firstly, the size of the leading edge vortex at $\theta = 160^\circ$ appears to be slightly larger with the addition of turbulence, and its position is slightly upstream compared to the laminar

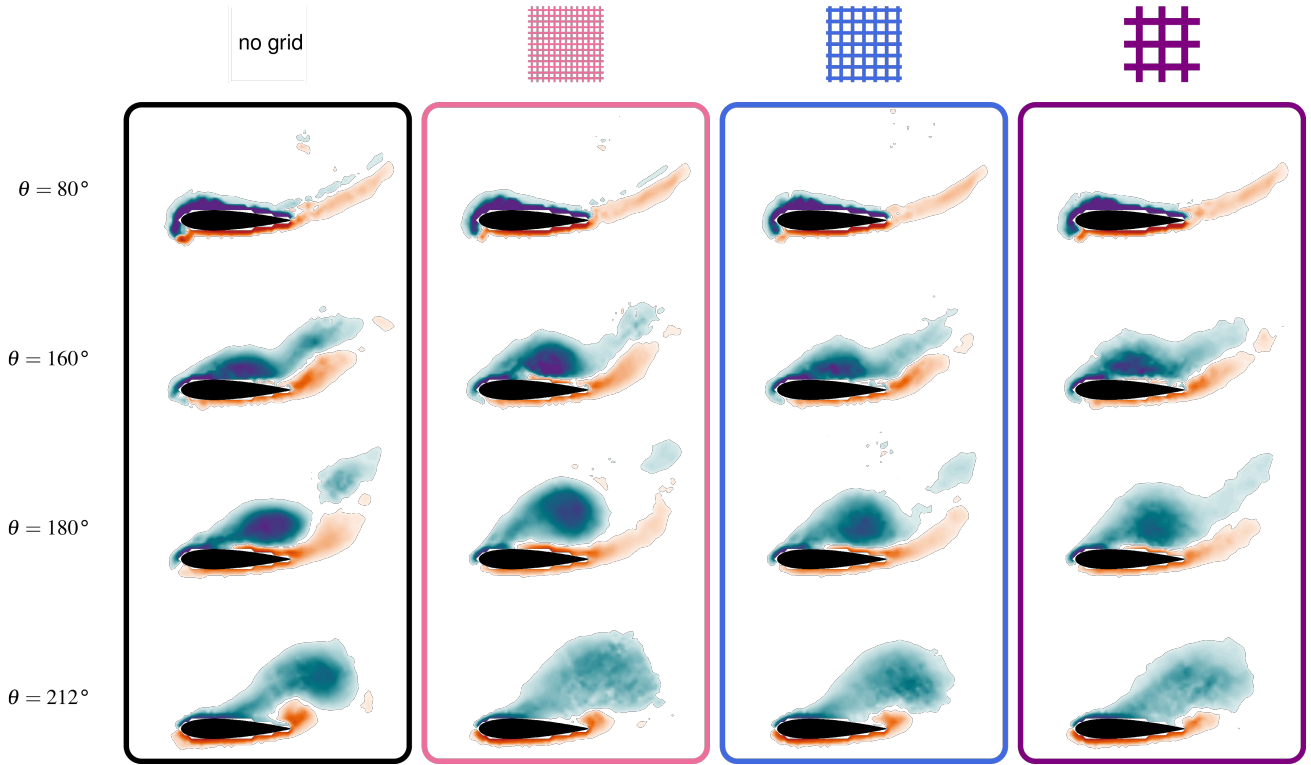


Figure 5: Phase-averaged vorticity plots at four phases during the rotation of the turbine. Green-blue indicates clockwise vorticity, orange-red anti-clockwise.

case. These physical changes to the leading edge vortex appear to have no discernible difference to the overall performance of the turbine, neither in the power output nor the total force. The most noticeable impact of the freestream turbulence, is the diffusion of the leading edge vortex during the rotation. As the turbulence levels increase, going from left to right in fig. 5 for the $\theta = 180^\circ$ phase, the leading edge vortex is increasingly diffuse. At this phase, the largest mesh size grid, producing 12% turbulence intensity levels in the flow, has the most diffuse leading edge vortex. As the blade moves to $\theta = 212^\circ$, the leading edge vortex is now diffuse for all the turbulent freestream cases.

Although the leading edge vortex is more diffuse under freestream turbulence, we also observe that the standard deviation of the total force has increased. As these are the phase-averaged vorticity plots, the diffusion can be due to increased viscous diffusion or due to cycle-to-cycle variations in the position of the vortex. However, one can postulate that if the leading edge vortex is larger, and is subjected to a turbulent flow whose integral scale is of the order of these structures, it is likely to be moved around in the vicinity of the blade which would lead to larger fluctuations of the total force.

The diffusion of the leading edge vortex, which has negligible effect on the average performance of a single blade, could very well have a positive influence on a vertical axis turbine comprised of multiple blades. The flow structures generated by the upwind blade, once shed, would interact with the downstream blades, especially during their power generation phase of rotation. If these structures are weaker and more diffuse, they could have less detrimental effects on the performance. This would be interesting to investigate in future work.

CONCLUSION

We investigated the performance of a single bladed vertical axis turbine at a Reynolds number of $Re \approx 50000$. Freestream turbulence was introduced with the addition of three regular, square-type grids at the start of the test section, having a mesh size of 45 mm, 90 mm and 180 mm. With increasing mesh size, the grids created turbulence intensity levels of 3%, 6%, and 12%, respectively, at the location where the turbine was located. The integral scale was found to be roughly 38 mm, 40 mm, and 57 mm, for the 45 mm, 90 mm and 180 mm mesh size grids, respectively. These integral scales range from roughly half the chord size of the blade ($c = 60$ mm), to approximately the size of the chord.

Under laminar conditions, the turbine has the largest power output at a tip speed ratio of $\lambda = 3$. With the addition of freestream turbulence, no appreciable change in power coefficient was observed at that particular tip speed ratio. For lower tip speed ratios, the effects of freestream turbulence were more pronounced. At $\lambda = 2.5$, the power coefficient increased by roughly 30% with a freestream turbulence level of 12%. The increase in power output comes at the cost of increased standard deviation of the total force, which increased by up to a factor of three for the highest turbulence case.

The phase-averaged flow around the blade suggests that the main reason for the increase in power output could be the slight change in location where the trailing shear layer leaves the blade, which would increase the effective angle of attack. Higher resolution measurements closer to the surface of the blade would need to be taken to fully understand these changes. Nevertheless, our measurements revealed that freestream turbulence was able to modify the large leading edge vortex that is formed during the rotation of the blade. This leading edge vortex grows to cover roughly half of the chord in the laminar case. With the addition of freestream

turbulence, this vortex is diffused, and slightly larger in size. WE postulate that this, combined with its interaction with the largest structures in the turbulent flow, could explain the increase in fluctuations of the total force. The diffusion of the leading edge vortex, which would eventually shed and advect downstream, could in turn have a beneficial effect on a multi-bladed turbine. This is left for future study.

REFERENCES

- Ahmadi-Baloutaki, M., Carriveau, R. & Ting, D.S-K. 2015 Performance of a vertical axis wind turbine in grid generated turbulence. *Sustainable Energy Technologies and Assessments* **11**, 178–185.
- Belabes, B. & Paraschivoiu, M. 2021 Numerical study of the effect of turbulence intensity on vawt performance. *Energy* **233**, 121139.
- Damiola, L., Siddiqui, M.F., Runacres, M.C. & De Troyer, T. 2023 Influence of free-stream turbulence intensity on static and dynamic stall of a naca 0018 aerofoil. *Journal of Wind Engineering and Industrial Aerodynamics* **232**, 105270.
- Hoffmann, J.A. 1991 Effects of freestream turbulence on the performance characteristics of an airfoil. *AIAA Journal* **29** (9), 1353–1354.
- Kumar, R., Raahemifar, K. & Fung, A.S. 2018 A critical review of vertical axis wind turbines for urban applications. *Renewable and Sustainable Energy Reviews* **89**, 281–291.
- Le Fouest, Sébastien & Mulleners, Karen 2022 The dynamic stall dilemma for vertical-axis wind turbines. *Renewable Energy* **198**, 505–520.
- Molina, A.C., De Troyer, T., Massai, T., Vergaerde, A., Runacres, M.C. & Bartoli, G. 2019 Effect of turbulence on the performance of vawts: An experimental study in two different wind tunnels. *Journal of Wind Engineering and Industrial Aerodynamics* **193**, 103969.
- Möllerström, E., Ottermo, F., Goude, A., Eriksson, S., Hylander, J. & Bernhoff, H. 2016 Turbulence influence on wind energy extraction for a medium size vertical axis wind turbine. *Wind Energy* **19** (11), 1963–1973.
- Nedić, J & Tavoularis, S 2016 Measurements of passive scalar diffusion downstream of regular and fractal grids. *Journal of Fluid Mechanics* **800**, 358–386.
- Peng, H.Y. & Lam, H.F. 2016 Turbulence effects on the wake characteristics and aerodynamic performance of a straight-bladed vertical axis wind turbine by wind tunnel tests and large eddy simulations. *Energy* **109**, 557–568.
- Peng, H.Y., Lam, H.F. & Liu, H.J. 2019 Power performance assessment of h-rotor vertical axis wind turbines with different aspect ratios in turbulent flows via experiments. *Energy* **173**, 121–132.